ARTICLE

Evolution of local strain in Ag-deposited monolayer MoS_2 modulated by interface interaction

Yinghui Sun,†[a] Yan Aung Moe,†[a] Yingying Xu,[a] Yufei Sun,[b] Xuewen Wang,[b] Fangtao Li,[a] Kai Liu,[b] and Rongming Wang*[a]

[a] Beijing Advanced Innovation Center for Materials Genome Engineering, Beijing Key Laboratory for Magneto-Photoelectrical Composite and Interface Science, School of Mathematics and Physics, University of Science and Technology Beijing, Beijing 100083, People's Republic of China

[b] State Key Laboratory of New Ceramics and Fine Processing, School of Materials Science and Engineering, Tsinghua University, Beijing 100084, People's Republic of China

Corresponding Author

*E-mail: rmwang@ustb.edu.cn

† Yinghui Sun and Yan Aung Moe have contributed equally to this work.

1. Layer identification of MoS_2 flakes on mica with Raman and PL measurements.

The Raman and PL measurements were done for layer identification of MoS_2 flakes before Ag deposition on every kind of substrates. The results of MoS_2 flakes on mica are shown in Figure S1.

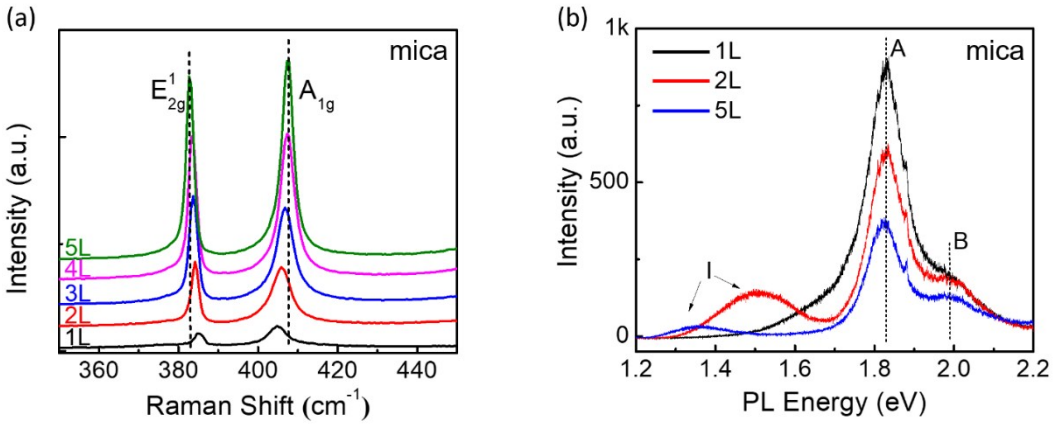

Fig. S1 (a) The Raman spectra of MoS_2 flakes on mica substrate from monolayer to pentalayer showing the characteristic E^1_{2g} and A_{1g} Raman modes, which evolve in different directions with the increasing thickness. (b) The PL spectra of monolayer, bilayer, and pentalayer MoS_2 on mica substrate. The notation "I" indicates the PL peak associated with the indirect-bandgap transition in few-layer MoS_2. "A" and "B" represent the PL peaks associated with the direct-bandgap transitions at K (K′) point [1, 2], and the energy difference between the "A" and "B" peaks corresponds to the splitting at the top of valence band due to the strong spin-orbital coupling.

2. Raman spectra of the pure substrates for the references for Raman peak positions.

The Raman spectra of the substrates were measured to clearly distinguish the Raman peaks from the Ag-MoS_2 heterostructures and the substrates themselves, and also for the purpose of data calibration in the measurements of different time periods.

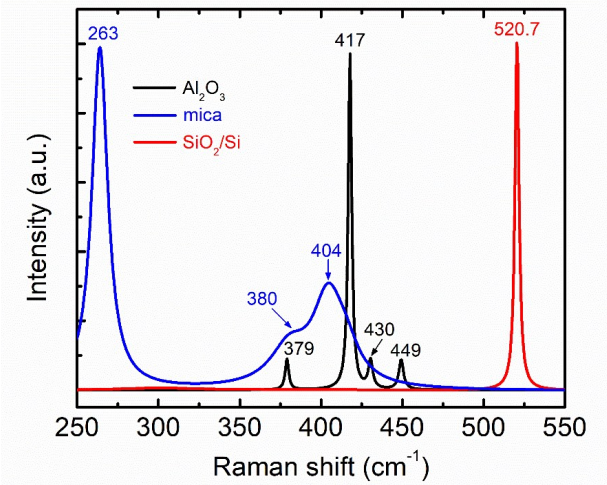

Fig. S2 The Raman spectra of pure Al_2O_3 (black), mica (blue) and SiO_2/Si (red) substrates. The scale in Y-axis is arbitrary and the spectra are normalized to their respective strongest peak between 250 cm^{-1} and 550 cm^{-1}.

3. Morphologies of the Ag nanostructures on MoS_2 supported by different substrates.

After the deposition of Ag by e-beam evaporation with a nominal thickness of ~3 nm, the morphology of the samples was characterized by scanning electron microscope (SEM, SUPRA 55VP) under a low work voltage of 1 kV. Ag forms dendrite nanostructures on MoS_2 as shown in Figure S3. The morphologies of Ag dendrites on 1L MoS_2 are similar on different substrates (Figs. S3a-c). The Ag dendrites on 1L MoS_2 are found to be smaller in width as compared with those on few-layer MoS_2. Apart from the influence of layer number on the growth of metal nanostructures [3], the formation of Ag dendrites seems to be affected by the strength of interface interaction. The morphology differences for Ag dendrites on 1L, 2L and 3L MoS_2 supported by Al_2O_3 substrate are quite subtle (Fig. S3a), while the morphology difference in the case of 1L and 2L MoS_2 on mica substate is quite distinct (Fig. S3c).

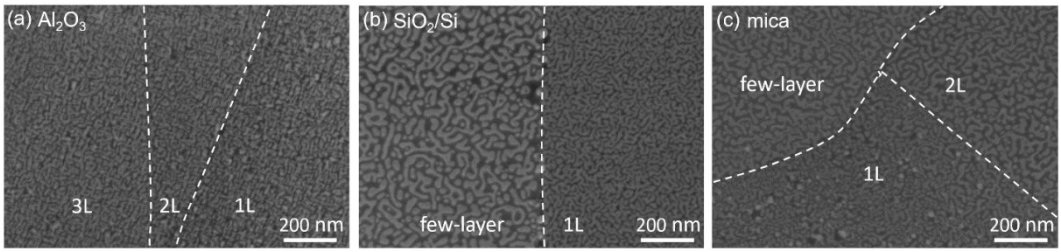

Fig. S3 SEM images of Ag-deposited 1L and few-layer MoS_2 on (a) Al_2O_3, (b) SiO_2/Si and, (c) mica substrates. The contrast of the images for Ag nanostructures on Al_2O_3 and mica substrates are lowered because of their intrinsic poor conductivity.

4. Determination of mica surface crystal orientation and composition.

Referring to Fig. S4a, the mica we used was found to have a monoclinic crystalline structure comparing to the standard card with the normal crystalline orientation along the <001> direction. Fig.S4c shows the XPS spectra of mica, with a detailed analysis of each peak; the content of each element in mica can be semi-quantitatively determined. Its chemical formula can be written as $KAl_2[AlSi_3O_{10}][OH]_2$.

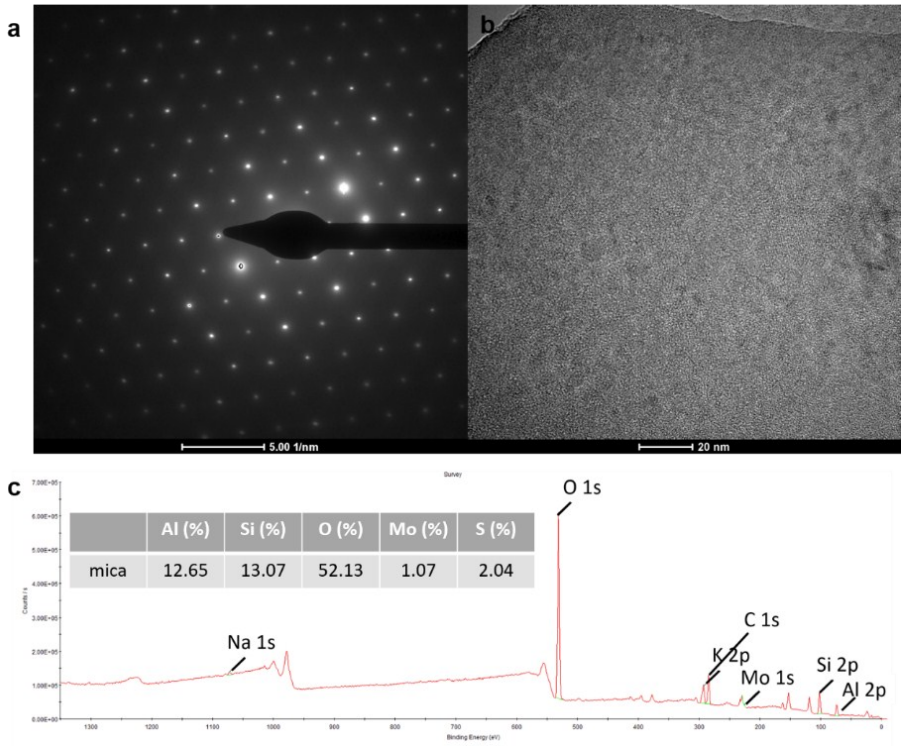

	Al (%)	Si (%)	O (%)	Mo (%)	S (%)
mica	12.65	13.07	52.13	1.07	2.04

Fig. S4 (a) Diffraction image and (b) SEM image of mica, demonstrating a monoclinic crystal of space group C2 with a (001) crystal plane, whose orientation is in the <001> direction perpendicular to the crystal plane. (c) XPS measurement showed that the chemical formula of the mica used is $KAl_2[AlSi_3O_{10}][OH]_2$.

5. Evolution of Raman spectra for Ag-deposited 2L MoS_2 on different kinds of substrates.

Another interesting phenomenon with respect to Al_2O_3 substrate is the maintenance of the strain in 2L MoS_2 which addresses to the strong interaction from Al_2O_3 surface. Besides the SERS effect, Ag dendrites can also induce the Raman peak splitting of E_{2g}^1 mode in 2L MoS_2, termed as $E_{2g}^{1'}$ peak. The evolution of $E_{2g}^{1'}$ Raman peak for the Ag-deposited 2L MoS_2 on the three substrates is respectively presented in Figs. S5a-S5c. With elapsed time, the relative intensity of $E_{2g}^{1'}$ Raman peak is distinctly reduced for Ag-2L MoS_2 samples on SiO_2/Si and mica substrates (indicated by the red arrows in Figs. S5b and S5c). The $E_{2g}^{1'}$ Raman peak evolved into a shoulder peak after 72 days for the sample on SiO_2/Si, while it totally disappeared after 48 days for the sample on mica. In contrast, the relative intensity of $E_{2g}^{1'}$ peak is nearly unchanged for that on Al_2O_3 substrate (indicated by the red arrows in Fig. S5a). Because the evolution of $E_{2g}^{1'}$ peak in intensity and position may reflect the change of interfacial strain, the results indicate that Ag-induced strain in 2L MoS_2 shows extraordinary stability on Al_2O_3 substrate. This excellent strain pinning effect of Al_2O_3 substrate for 2L MoS_2 is remarkable and can be attributed to the electron configuration at the surface of Al_2O_3, which the bottom layer of 2L MoS_2 interacts with.

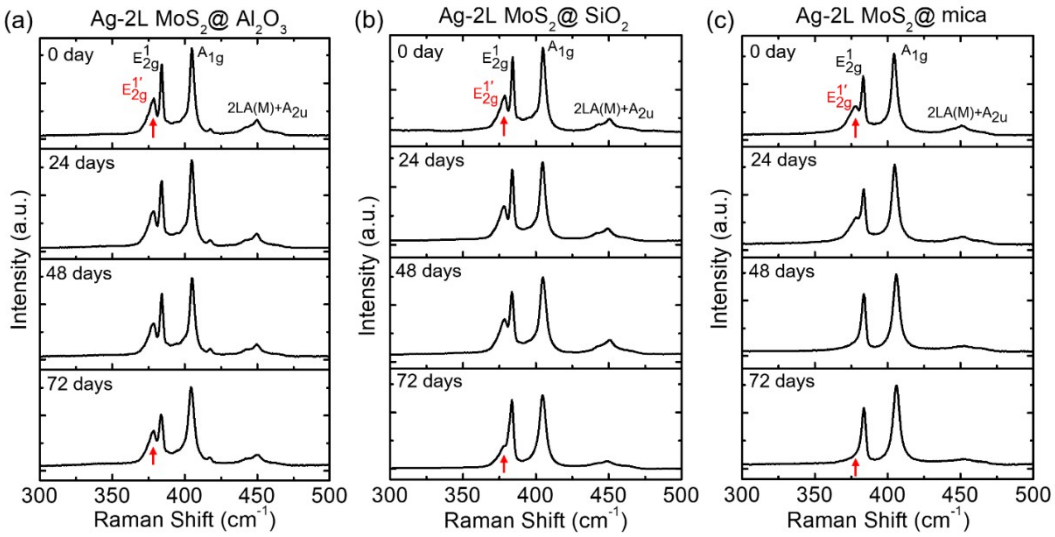

Fig. S5 Evolution of Raman spectra over time for Ag-deposited 2L MoS_2 on Al_2O_3 substrate (a), SiO_2/Si substrate (b), and (c) mica substrate. 2L MoS_2 on all three types of substrates undergoes Raman peak splitting after Ag deposition. The quenching rate of the splitting Raman peaks of $E_{2g}^{1'}$ modes differs, as indicated by the red arrows.

6. Measuring the surface roughness of the different substrates.

Because the surface roughness has a distinct influence on the MoS_2-substrate interaction and strain relaxation, the surface roughness for the three substrates were measured by using Bruker Multimode 8 in a peak-force tapping mode. The values of root-mean-square roughness (R_q) were 0.143 nm for Al_2O_3, 0.145 nm for SiO_2/Si, and 0.113 nm for mica substrate, respectively.

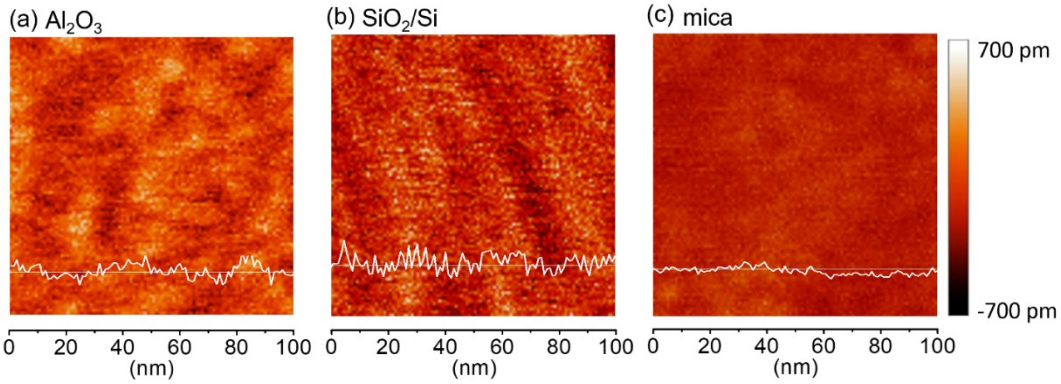

Fig. S6 Surface topographies and the line profiles for (a) Al_2O_3, (b) SiO_2/Si, and (c) mica substrates.

7. SEM images and Raman spectra of 1L MoS_2 deposited with 10-nm- and 20-nm-thick Ag.

SEM images of Ag-deposited 1L MoS_2 on the three kinds of substrates are shown in Fig. S7(a)-(c). A large number of pinholes are clearly observed, indicating that the 10-nm Ag film cannot fully cover the MoS_2 surface. Therefore, we tried to deposit a thicker Ag film with a thickness of 20 nm on 1L MoS_2. SEM images in Fig. S7(d)-(f) show that the density of pinholes is greatly reduced, and the Ag film almost fully cover the MoS_2 surface. Raman spectra are measured at the same ambient conditions as shown in Fig. S7(g)-(i). Because the splitting of E^1_{2g} Raman peak can be regarded as the dominant indicator of local strain at the metal-MoS_2 boundary, we focus on the Raman feature of this mode. Compared with the Raman spectrum of pristine MoS_2 on Al_2O_3 (black curve in Fig. S7(g)), the Raman splitting can still be detected for 1L MoS_2 deposited with 10-nm-thick Ag on Al_2O_3. Similar Raman splitting is also observed for the samples on SiO_2/Si and mica substrates (red curves in Fig. S7(h) and (i)).

Compared with the samples deposited with 10-nm-thick Ag, the 1L MoS_2 deposited with 20-nm-thick Ag on the three substrates has much weakened and broadened E^1_{2g} Raman peaks (green curves in Fig. S7(g)-(i)). The peak shoulders around the position of $E^{1'}_{2g}$ mode may be attributed to the remained small amount of pinholes existed on MoS_2.

These results can be explained by the Volmer-Weber island growth mode of Ag on MoS_2, as sketched in Fig. S7(j). In the pinholes of Ag film, the focused laser can directly illuminate the MoS_2, which contributes to the pristine E^1_{2g} peak. At the positions within ~1 nm around the edge of the Ag dendrites, the detected Raman signal contributes to the redshifted $E^{1'}_{2g}$ mode. Therefore, we can observe the Raman splitting in the spectra of 10-nm-thick Ag deposited MoS_2. Even though much less pinholes can be observed from the top view of SEM images when the thickness of Ag is further increased, the vacuum cavities cannot be avoided due to the Volmer-Weber island growth mode. The focused laser can pass through the surficial Ag thin layer and

illuminate the MoS_2 beneath. Therefore, the Raman peaks of E^1_{2g} and $E^{1'}_{2g}$ modes can still be observed but with a much reduced intensity for the samples deposited with 20-nm-thick Ag.

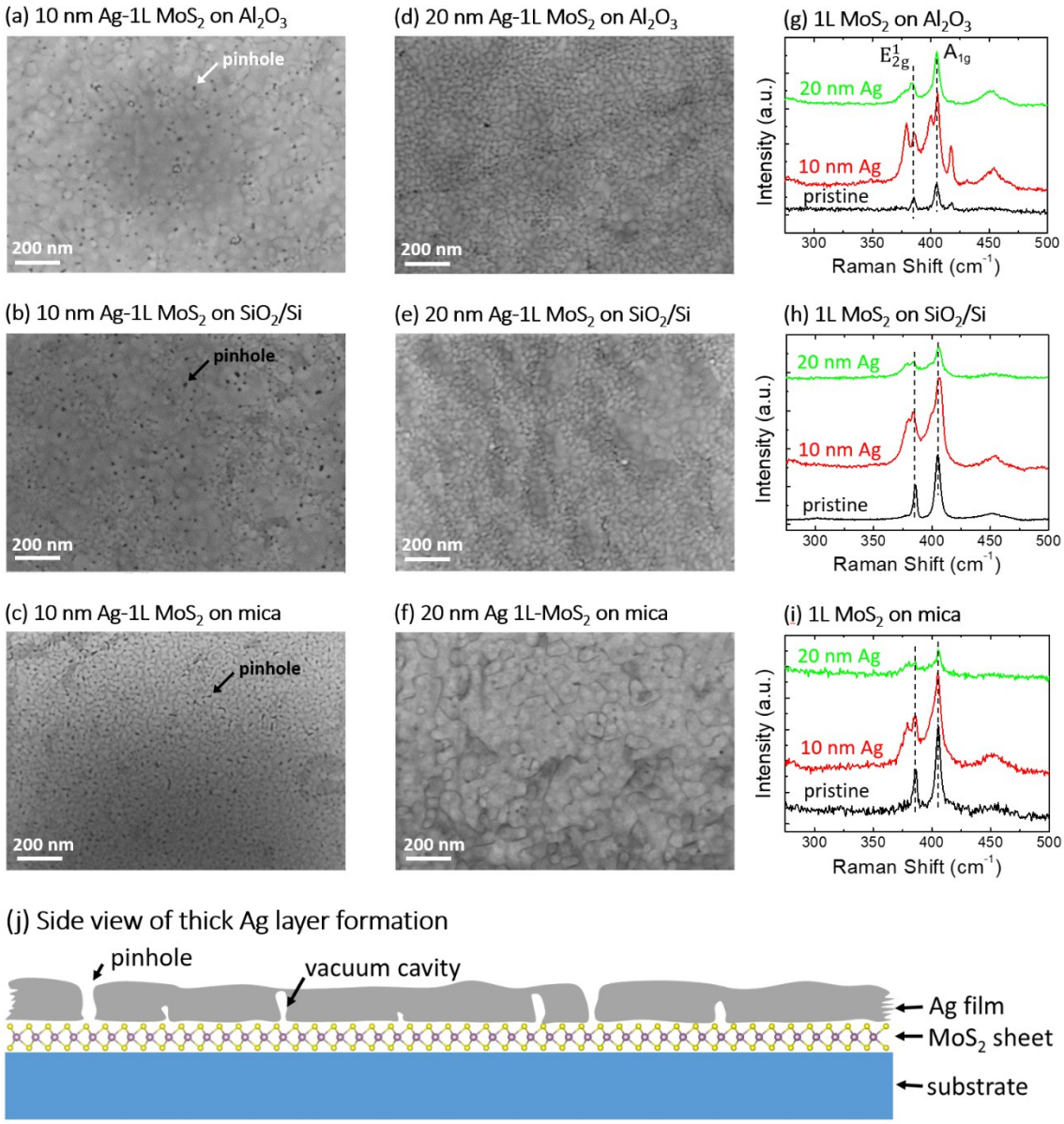

Fig. S7 SEM images and Raman spectra of Ag-deposited 1L MoS_2 on the three kinds of substrates. (a) SEM image of 10-nm-Ag deposited 1L MoS_2 on Al_2O_3; (b) SEM image of 10-nm-Ag deposited 1L MoS_2 on SiO_2/Si wafer; (c) SEM image of 10-nm-Ag deposited 1L MoS_2 on mica; (d) SEM image of 20-nm-Ag deposited 1L MoS_2 on Al_2O_3; (e) SEM image of 20-nm-Ag deposited 1L MoS_2 on SiO_2/Si wafer; (f) SEM image of 20-nm-Ag deposited 1L MoS_2 on mica; (g) Raman spectra of 0, 10, 20 nm-Ag deposited 1L MoS_2 on Al_2O_3; (h) Raman spectra of 0, 10, 20 nm-Ag deposited 1L MoS_2 on SiO_2/Si wafer; (i) Raman spectra of 0, 10, 20 nm-Ag deposited 1L MoS_2 on mica; (j) Schematic illustration of the side view of the interface between a thick Ag film deposited on 1L MoS_2 on a substrate.

REFERENCES

1. Mak KF, Lee C, Hone J et al (2010) Atomically thin MoS_2: A new direct-gap semiconductor. Phys Rev Lett 105: 136805
2. Splendiani A, Sun L, Zhang Y et al (2010) Emerging photoluminescence in monolayer MoS_2. Nano Lett 10: 1271-1275
3. Zhou H, Qiu C, Liu Z et al (2010) Thickness-dependent morphologies of gold on n-layer graphenes. Journal of the American Chemical Society 132: 944-946